How to cite: *Angew. Chem. Int. Ed.* **2022,** *61,* e202207018
International Edition: doi.org/10.1002/anie.202207018
German Edition: doi.org/10.1002/ange.202207018

Ether Electrolyte Degradation

Phase Transfer-Mediated Degradation of Ether-Based Localized High-Concentration Electrolytes in Alkali Metal Batteries

Xiaojuan Chen[+], Lei Qin[+], Jiaonan Sun, Songwei Zhang, Dan Xiao, and Yiying Wu**

Abstract: Localized high-concentration electrolytes (LHCEs) have attracted interest in alkali metal batteries due to the advantages of forming stable solid-electrolyte interphases (SEIs) on anodes and good chemical/electrochemical stability. Herein, a new degradation mechanism is revealed for ether-based LHCEs that questions their compatibility with alkali metal anodes (Li, Na, and K). Specifically, the ether solvent reacts with alkali metals to generate solvated electrons (e_s^-) that attack hydrofluoroether co-solvents to form a series of byproducts. The ether solvent essentially acts as a phase-transfer reagent that continuously transfers electrons from solid-phase metals into the solution phase, thus inhibiting the formation of stable SEI and leading to continuous alkali metal corrosion. Switching to an ester-based solvating solvent or intercalation anodes such as graphite or molybdenum disulfide has been shown to avoid such a degradation mechanism due to the absence of e_s^-.

To meet the requirements of high-energy-density batteries, alkali metal anodes are desirable due to their high theoretical specific capacities and low redox potentials.[1] For these highly reactive anodes, it is vital to design stable electrolytes. Localized high-concentration electrolytes (LHCEs) have been considered to be a promising electrolyte choice because this design inherits the advantage of high-concentration electrolytes (HCEs) with large electrochemical windows while minimizing the disadvantages of HCEs in viscosity, wettability and cost.[2,3] In an LHCE, a solvating solvent (such as dimethoxyethane, DME) is used to dissolve a high concentration of alkali salts, which is then diluted by a low-polarity inert co-solvent such as a highly fluorinated ether (HFE) to reduce viscosity without altering the solvation structure.[4]

Ether-based solvents are the popular choices for HCEs and LHCEs because of the strong solvating power for dissolving alkali salts.[5] However, it has long been known that chelating ethers such as DME, tetraethylene glycol dimethyl ether (TEGDME), and crown ether can dissolve alkali metals, forming blue solutions.[6] The blue species consist of metal anions (M^-) in a dynamic equilibrium with solvated electrons (e_s^-).[7,8] M^- and e_s^- are highly reactive nucleophiles that cleave C–O bonds in ethers.[7] They have also been utilized in the reduction reactions of olefins,[9–11] nitriles,[12] oligopeptides,[13] and nitrogen.[14] The blue solution formed by dissolving potassium (K) in DME was able to initiate the anionic polymerization of styrene.[15] Considering the high reactivities of M^- and e_s^-, it raises the question of whether the ether-based LHCEs are truly compatible with alkali metals, especially for sodium (Na) and K. Recently, Popovic has demonstrated that the porous solid-electrolyte interphases (SEIs) formed on metal anodes in ether-based electrolytes are liquid/solid composites that allow for ion transport and further SEI growth.[16,17] The non-passivating nature of such SEIs is detrimental to the performance of alkali metal batteries. In addition, recent reports speculate that the "inert" HFE may participate in the buildup of anode electrolyte interphase in alkali metal secondary battery system by the surface analyses characterization (Table S1). However, the detailed electrolyte decomposition process remains ambiguous.

In this work, a degradation phenomenon of alkali metal anodes in ether-based LHCE was observed in metal-Cu half cells. The intrinsic stabilities of alkali metals were then systematically investigated against the specific components in the LHCE, and the underlying reaction mechanism was proposed. It is observed that the K and Na metal exhibit severe corrosion in DME/HFE mixture or LHCE solution while remaining relatively stable in the pure HFE solution. It is further proposed that DME can continuously transfer electrons from the alkali metals into the solution and thus prevent the formation of SEIs on alkali metal anodes. Compared with the metal-electrolyte contact, the M^-/e_s^- can increase the contact between electrons and HFE, thus facilitating the HFE decomposition. The C–O cleavage and defluorination reactions induced by M^-/e_s^- deconstruct HFE into H_2, F^-, $CF_3CH_2O^-$ and sp^2 carbon. However, this phenomenon is oblivious in the ester/HFE mixture possibly due to the incapability of forming M^-/e_s^- in ester solvents.

[*] X. Chen,[+] Prof. D. Xiao
College of Chemical Engineering, Sichuan University
Chengdu 610065, (P. R. China)
E-mail: xiaodan@scu.edu.cn

Dr. L. Qin,[+] Dr. J. Sun, S. Zhang, Prof. Y. Wu
Department of Chemistry and Biochemistry, The Ohio State University
100 West 18th Avenue, Columbus, OH 43210 (USA)
E-mail: wu@chemistry.ohio-state.edu

[+] These authors contributed equally to this work.

Finally, the K-intercalated graphite and molybdenum disulfide (MoS_2) are proposed to be promising anode alternatives to metallic K in ether-based LHCEs due to the absence of M^-/e_s^-.

2,2,2-Trifluoroethyl 1,1,2,2-tetrafluoroethyl ether (TFTFE) is selected as a representative HFE co-solvent to dilute the parent HCEs for preparing the LHCEs. K–Cu half cells were assembled with an ether-based LHCE while the cell with an HCE was used as the control sample (Figure 1a, b). Both cells delivered high average coulombic efficiencies above 95 % in the first 100 cycles (Figure S1a), but the cycled anodes showed distinct appearances (insets of Figure 1a, b). Compared to the sparse grey residue on the K surface in the HCE, the cycled anode in the ether-based LHCE exhibited a black surface with rough morphology, which implied severe K metal corrosion. The same anode degradation phenomenon was also observed on cycled Na and lithium (Li) anodes with the ether-based LHCEs (Figure 1c, d) despite the decent lifespans and high coulombic efficiencies of the metal-Cu half cells (Figure S1b, c). For investigating the formed byproducts, the surface layer of the cycled K metal disk was scratched and dissolved into D_2O for nuclear magnetic resonance (NMR) tests. As shown in Figure 1e, f, a new quartet ($\sigma = 4.0$ ppm) in the ^{1}H NMR together with the singlet ($\sigma = -76$ ppm) in ^{19}F NMR spectra are assigned to the methylene and terminal CF_3 in trifluoroethanolate ($CF_3CH_2O^-$). Such species is further verified by the standard sample of 2,2,2-trifluoroethanol (TFE, CF_3CH_2OH) in Figure S2. This fragment should come from the C–O cleavage decomposition of TFTFE on the K metal surface upon long-term cycles, which is not consistent with previous thoughts on its intrinsic "inertness".[3] The formation of acetate (CH_3COO^-, $\sigma = 1.9$ ppm) is due to the DME decomposition. Furthermore, the same byproducts were detected on the cycled Na and Li anodes in ether-based LHCEs (Figure 1g, h).

To explore the effects of different components in the LHCE system, the stability of Li, Na, and K metals was examined under three different conditions: 1) pure TFTFE solvent (denoted as #1_Li/Na/K), 2) mixed solution of TFTFE and DME (denoted as #2_Li/Na/K), and 3) LHCE consisting of TFTFE and DME with LiFSI, NaFSI, or KFSI as the salt (denoted as #3_Li/Na/K) (see Table S2 for details). For Li, there is no noticeable color change on the Li metal surface in any of these three reactions, indicating its chemical stability against different components of LHCE (Figure S3a–c). Note that there is no apparent reaction in #1_K (Figure S3g), but a severe corrosion phenomenon could be observed on the K metal in #2_K (Figure S3h) or other ratios of TFTFE/DME (Table S3). Some brown intermediates were generated immediately, and black products were formed in #2_K after total consumption of metallic K. A visible smoke was formed with heat release during the reaction (Supporting Video). Although there was no apparent change on the K surface in #3_K initially (Figure S3i), black spots appeared at the 12th minute, followed by a harsh corrosion reaction that converted K metal to black byproducts. Similar corrosion reactions could also be observed on Na metal in the ether-based LHCE and the TFTFE/DME mixture but at a slower speed (Figure S3e and f). In addition, Na metal is demonstrated to be unstable to TFTFE, and some white particles were formed on the Na surface after 48 hours (Figure S3d). Different from the observation in the ether solvent case, both K and Na metals kept more stable against the TFTFE/ester mixture without detectable byproducts even after 24 hours (Figure S4).

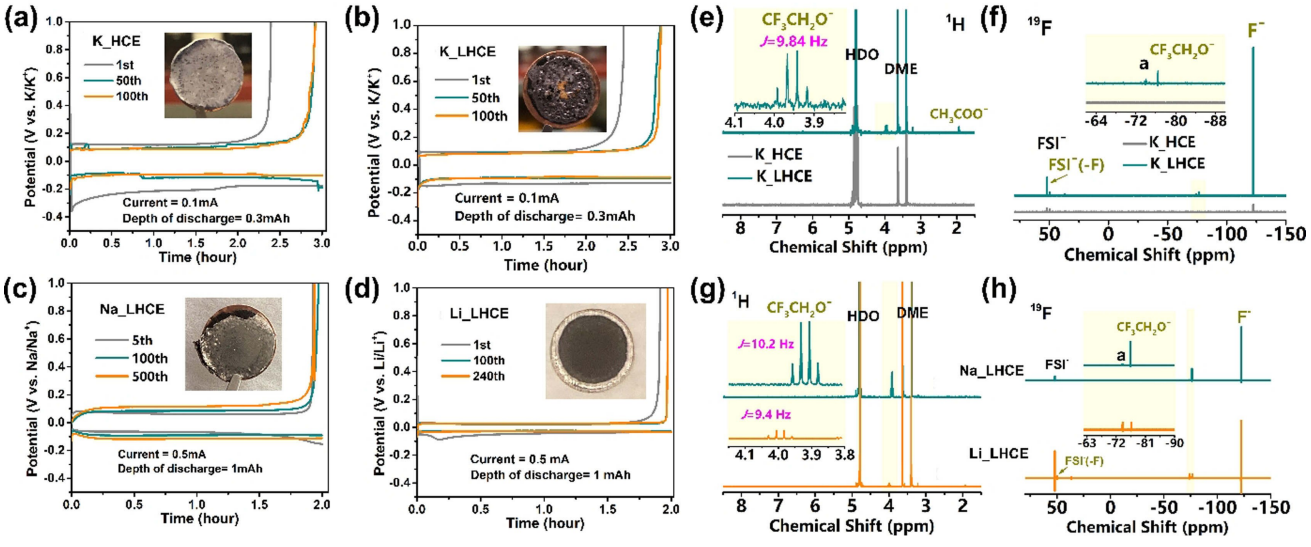

Figure 1. a)–d) The electrochemical performances of the alkali metal-Cu half cells with the recipes of LHCE and HCE, and optical images of the cycled metal anodes (insets). The surface layer of the cycled metal disk was scratched and dissolved into D_2O for the NMR tests. The results are shown in the e), g) ^{1}H and f), h) ^{19}F NMR spectra.

Given the distinct metal (Na and K) reactivity in TFTFE/DME and TFTFE/ester cases, as well as the lack of severe corrosion in pure TFTFE, it is reasonable to associate the metal corrosion with the differences between DME and ester.

To investigate the underlying corrosion mechanism, the K system was selected to analyze the reaction products in the forms of solid, gas, and solution phases. Gas chromatography (GC) tests were conducted to monitor the possible gaseous products during the reaction. From the raw data in Figure S5 and the corresponding histogram in Figure 2a, the gas products mainly consisted of hydrogen (H_2), CH_4, and C_2H_4. After normalizing the evolved gas amounts in #2_M and #3_M to #1_M, all the Li reactions show negligible change. In comparison, about 2500 times of gas amount was generated when DME participated in the reaction of K and TFTFE, which is consistent with the observation of the severe metal degradation in #2_K. Furthermore, the addition of KFSI salt was unable to stop the K corrosion with a large amount of gas formed in #3_K. A similar trend is observed when the gas amounts in #2_K and #3_K are normalized to #4_K, which represents the side reaction between bare K and DME. Owing to the Na corrosion being limited on the surface, the evolved gas change is not significant. In general, the overall changing trend for the metallic K or Na in different conditions indicated that the catastrophic decomposition of TFTFE is triggered in the presence of ether solvent, and the salt addition can slow down the side reactions to some extent.

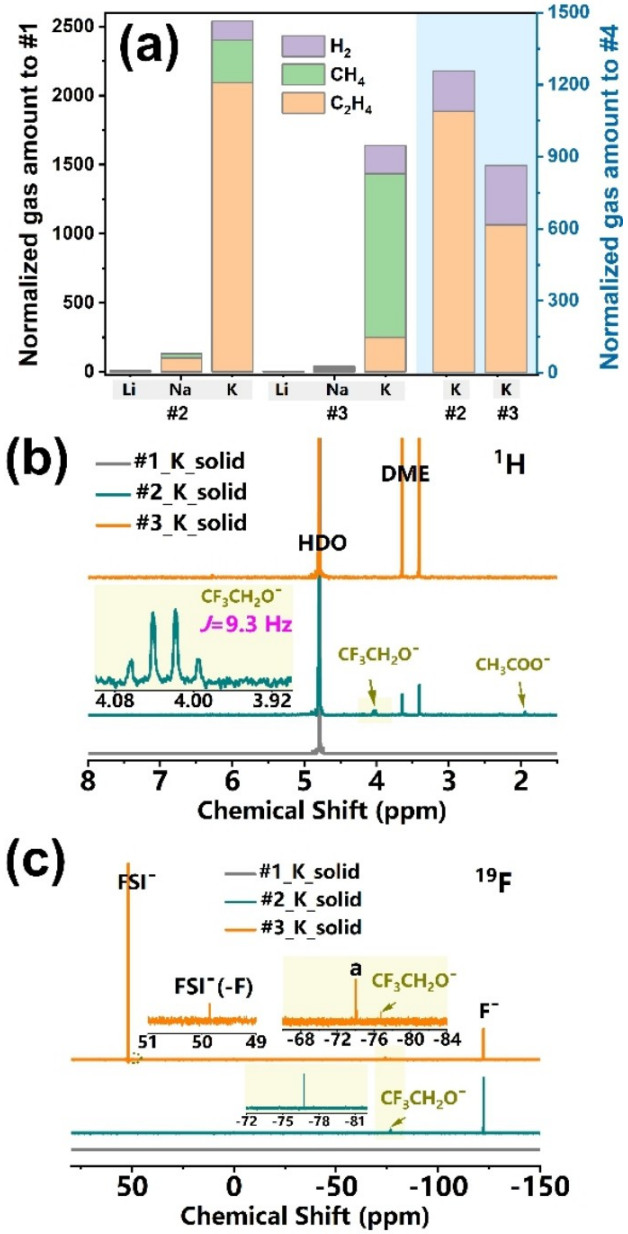

Figure 2. a) The normalized gas evolution amounts of #2_M and #3_M samples based on #1_M (M = Li, Na, or K) or #4_K. b), c) The NMR spectra of the series of K reaction solid products; D_2O was used for NMR tests.

After the reaction, the resulting solid products were collected and dissolved in D_2O for NMR tests. A filter was used to remove insoluble solids (Figure S6a), which were characterized by Raman and Fourier Transform Infrared Spectroscopy (FTIR) (vide infra). As evidenced in Figure 2b,c, the typical byproduct of $CF_3CH_2O^-$ was detected in the mixture of co-solvent and DME for the #2_K sample. The TFTFE decomposition in the #2_K sample is further verified from the F^- signal (KF, $\sigma = -122.0$ ppm) in ^{19}F NMR and KF solid from the XRD pattern (Figure S6b). The $CF_3CH_2O^-$ signal is also visible in the #3_K sample. In comparison, no fluoride or trifluoroethanolate components are detected on the 1#_K sample, indicating good stability of TFTFE against metallic K. The insoluble black solid product left in #2_K was identified as the conjugated carbon products due to the assignment of sp^2 bond carbon species through Raman and FTIR analyses (Figure S6c, d). After the above analyses, it is concluded that the solid products include sp^2 carbon, KF, CF_3CH_2OK, and CH_3COOK.

Based on the characterization of solid products and analyses on gas components, we propose that the decomposition mechanism for TFTFE is related to e_s^- and/or potassides (K^-). As mentioned in the introduction, it has been long known that K metal can dissolve in DME forming K^+, K^-, and e_s^- in a dynamic equilibrium.[18–24] e_s^- were detected by electron spin resonance test in K-tetrahydrofuran (THF)/crown-ether in prior studies, but only a weak spin resonance absorption line was observed for K-DME at −80 °C.[25] Nevertheless, the anionic polymerization was initiated by the K^-/e_s^- released from the K-DME system.[15] In addition, the K^-/e_s^- could induce a fission of the C–O bonds in THF and crown ether with the liberation of C_2H_4.[7] Hence, in our LHCE system, K metal can be dissolved in DME-containing solutions with K^-/e_s^- release. The formed K^-/e_s^- could reduce the acidic terminal proton of TFTFE molecules with H_2 release, just as proposed in Figure 3a. In pathway 1, the unshared pair of electrons on the resultant carbanion is then shared with the neighboring carbon to form the double bond with fluoride as the leaving group. In the environment of excess K^-/e_s^-, reductive polymerization and nucleophilic elimination can continuously occur to form the final black polymeric carbon.[15] These hypotheses can be

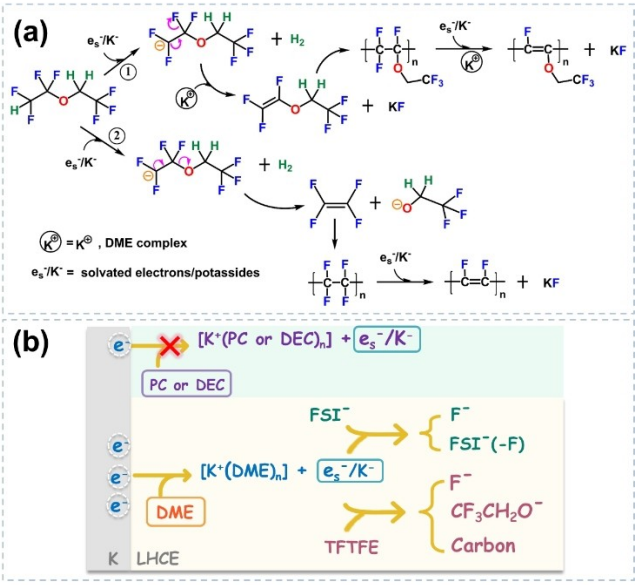

Figure 3. a) The possible decomposition pathways of the TFTFE under the attack of K^-/e_s^-. b) The distinct decomposition pathways in ether or ester solvents due to different capabilities for forming K^-/e_s^-.

further validated from the XPS spectra in Figure S7. There are no substantial differences in #2_K and #3_K solid products except for the KFSI salt species. The signals of C=C, C–C, C–O, C–F, and polymer species indicated that the reductive polymerization occurred with the conjugated carbon formation. In addition, the C–O bonds in TFTFE are also susceptible to nucleophilic attack,[24,26] as presented in pathway 2. The lone pair in the carbanion induces the double bond in tetrafluoroethylene while the C–O bond breaks with the leaving of the corresponding $CF_3CH_2O^-$ group. In the extremely basic condition with K^-/e_s^-, olefins in tetrafluoroethylene could also undergo polymerization to form fluoropolymers, and C_2F_4 is difficult to be detected. To verify this assumption, the generated gases of #2_K were injected into the C_6D_6 solution. As shown in Figure S8, the singlet of C_2H_4 is found at 5.25 ppm in the ^1H spectrum, but no C_2F_4 signal is shown in the ^{19}F spectrum. Instead, CH_2CF_2 (−81.76 ppm) was identified, and the possible formation pathway of CH_2CF_2 is proposed in Figure S9.

The above mechanism applies to LHCE that contains KFSI salt. As shown in Figure S3i, even though the K metal appeared stable without any color change during the first 12 minutes in #3_K, extensive black solid products still formed after 20 minutes. The FSI^- anions are proposed to be preferentially reduced on the metal surface at the beginning because only the defluorinated FSI^- species are detected in #3_K solid product with the reaction time of 2 minutes (Figure S10). This can be ascribed to the lower reduction potential and LUMO value of FSI^- than DME and TFTFE in an LHCE recipe.[26,27] Nevertheless, the formed byproduct layer cannot fully isolate the K from contacting with solvents. Any pit holes in this layer would allow the formation/accumulation of K^-/e_s^- in solution, thus triggering the dissociation of the TFTFE molecules. Note that the consumption of the K^-/e_s^- would shift the equilibrium to release more electrons from K metal into the solution until the total consumption of metal. In comparison, the ester molecules are susceptible to nucleophilic attack and unable to form K^-/e_s^-, resulting in limited solid–liquid contact between electrons and TFTFE. As a result, the TFTFE decomposition is unfavored in the ester case. The distinct routes in ether or ester solvents are compared and illustrated in Figure 3b.

To further elucidate the corrosion products growth mechanism, the above side reactions are terminated factitiously (see the details in Figure S11). In specific, a piece of partially corroded K metal with a KFSI_LHCE-derived SEI layer was rested in the fresh TFTFE/DME mixture (Figure S11a). The byproducts from the defluorination reaction of TFTFE could be observed and all the K was consumed in 5 minutes. This indicates the continuous proceeding of the side reactions and the porous property of the as-formed SEI derived from the KFSI_LHCE system. Notably, Popovic's recent studies have revealed the porous SEIs and further growth mechanism in metal anode cases with ether-based electrolytes.[16,17] The factor of porous SEI may also contribute to the K metal anode degradation in the ether-based LHCE system because it provides the chance for electrolyte penetration and facilitates K^-/e_s^- formation. As a result, the side reactions between the e_s^- and TFTFE are largely accelerated, and the formation of stable SEI is inhibited. In comparison, in pure TFTFE or DME solution (Figure S11b), the partially corroded K bulks maintained the integrity even after 2 days, and no sign of TFTFE decomposition is shown in the related NMR results (Figure S11c). The experiment results again demonstrate the instability of TFTFE against metallic K in the presence of DME solvent.

To directly prove the critical role of K^-/e_s^- in affecting the TFTFE stability, we first prepared blue K^-/e_s^- solution and then evaluated its reactivity with TFTFE (Figure 4a). Metallic K was firstly soaked into the TEGDME or 18-crown-6/THF solvent. As reported previously, these solutions enriched in K^-/e_s^- exhibit the characteristic dark blue color.[20,21,23] The obtained dark blue solution without K metal was quickly transferred into the TFTFE, and a yellowish color change was observed (Figure 4b). The ^{19}F NMR data verified that the TFTFE was defluorinated, with three new peaks detected at the upfield of the pristine TFTFE signals together with an F^- peak at −122 ppm. This is consistent with the observation in the NMR spectrum of #2_K liquid. Furthermore, no defluorination reaction was observed when aging the as-synthesized potassiated graphite (KC_8) or potassiated MoS_2 ($K_{0.4}MoS_2$) electrode in an LHCE solution due to the absence of K^-/e_s^- and the protection of stable and dense SEI (Figure 4c, d, Figure S12). The superior stability of TFTFE against KC_8 and $K_{0.4}MoS_2$ electrodes further elucidated the vital role of K^-/e_s^- in inducing TFTFE decomposition, which also highlights the potential application of graphite and MoS_2 anodes in an ether-based LHCE system. The analogous decomposition mechanism is also applied for Na as the same gases and solid products are detected (Figures S13). In comparison, no

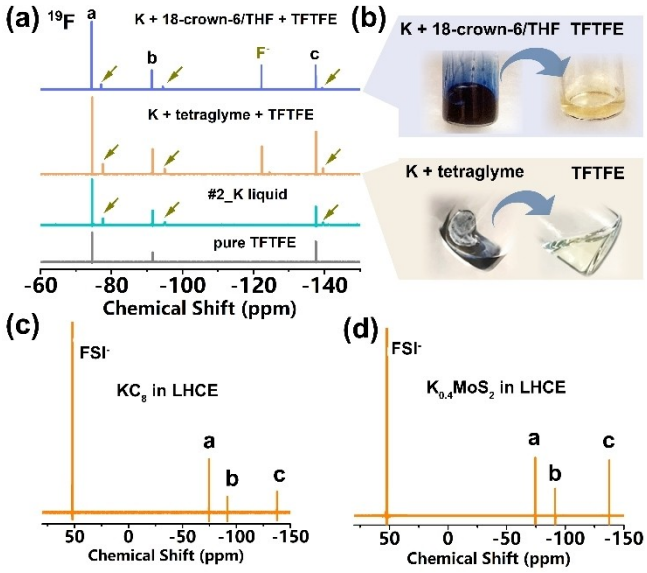

Figure 4. ^{19}F NMR spectra of a) the pristine TFTFE before and after adding K^-/e_s^-. The sample "#2_K liquid" represents the reacted liquid after aging K in TFTFE/DME mixture. b) Aging metallic K in 18-crown-6/THF or TEGDME solution followed by transferring the blue K^-/e_s^- solution into TFTFE. ^{19}F NMR spectra of the reacted liquids after aging c) KC_8 or d) $K_{0.4}MoS_2$ in the KFSI-based LHCE.

TFTFE decomposition fragments can be identified in Li series reactions (Figure S14), highlighting the chemical stability of Li metal against LHCE components. Unlike the static chemical reactions, the Li anode corrosion was triggered under the electrochemical cycling with a rich electron flow (Figure 1d). It requires special attention to the possible side reactions abovementioned because this may continuously consume the co-solvent and metallic anode in the ether-based LHCE during the long-term cycling of practical cells. Nevertheless, such a phenomenon is neglected due to the usage of excessive alkali metal in lab-scale coin-cell testing.

In summary, this work reports an uncharted HFE co-solvent decomposition and metal anode corrosion phenomenon in ether-based LHCE systems. Spectroscopic and GC analyses indicated that TFTFE exhibits the C–O bond breaking and defluorination process. TFTFE decomposition is revealed to be the result of a nucleophilic attack from K^-/e_s^-, which are transferred from the bulk solid metal to the liquid ether-based electrolyte. Alkali metal-Cu half cells were assembled, and the same severe corrosion was observed, which is a critical concern for practical batteries with limited metallic anodes and lean electrolytes. The graphite and MoS_2 anodes are proposed as potential candidates in ether-based LHCEs due to the absence of K^-/e_s^-. Another way to circumvent this decomposition is to use organic ester solvents. The incapability for forming K^-/e_s^- in ester solvents cannot trigger the hydrofluoroether deconstruction. The findings here would hopefully facilitate a better understanding of electrolyte chemistry and motivate the development of LHCEs for practical alkali metal secondary batteries.

Acknowledgements

The authors acknowledge funding support from the U.S. Department of Energy (Award No. DE-FG02-07ER46427) and the Ohio State University and Sichuan University for partial support of this work. X.C. acknowledges the financial support from the China Scholarship Council (CSC) under Grant No.201906240201. The authors thank Jingfeng Zheng and Ruiyang Lyu for many valuable discussions and thank Luke Schkeryantz for the manuscript polish.

Conflict of Interest

The authors declare no conflict of interest.

Data Availability Statement

The data that support the findings of this study are available from the corresponding author upon reasonable request.

Keywords: Alkali Metal Batteries · Co-Solvent Decomposition · Localized High-Concentration Electrolytes · Phase Transfer · Solvated Electrons

[1] S. Jiao, X. Ren, R. Cao, M. H. Engelhard, Y. Liu, D. Hu, D. Mei, J. Zheng, W. Zhao, Q. Li, N. Liu, B. D. Adams, C. Ma, J. Liu, J.-G. Zhang, W. Xu, *Nat. Energy* **2018**, *3*, 739–746.
[2] K. Dokko, N. Tachikawa, K. Yamauchi, M. Tsuchiya, A. Yamazaki, E. Takashima, J.-W. Park, K. Ueno, S. Seki, N. Serizawa, M. Watanabe, *J. Electrochem. Soc.* **2013**, *160*, A1304–A1310.
[3] J.-G. Zhang, W. Xu, J. Xiao, X. Cao, J. Liu, *Chem. Rev.* **2020**, *120*, 13312–13348.
[4] X. Ren, L. Zou, S. Jiao, D. Mei, M. H. Engelhard, Q. Li, H. Lee, C. Niu, B. D. Adams, C. Wang, J. Liu, J.-G. Zhang, W. Xu, *ACS Energy Lett.* **2019**, *4*, 896–902.
[5] O. Borodin, J. Self, K. A. Persson, C. Wang, K. Xu, *Joule* **2020**, *4*, 69–100.
[6] J. L. Down, J. Lewis, B. Moore, G. Wilkinson, *J. Chem. Soc.* **1959**, *209*, 3767.
[7] Z. Jedlinski, A. Stolarzewicz, Z. Grobelny, M. Szwarc, *J. Phys. Chem.* **1984**, *88*, 6094–6095.
[8] S. H. Glarum, J. H. Marshall, *J. Chem. Phys.* **1970**, *52*, 5555–5565.
[9] G. M. Whitesides, W. J. Ehmann, *J. Org. Chem.* **1970**, *35*, 3565–3567.
[10] H. W. Sternberg, R. E. Markby, I. Wender, D. M. Mohilner, *J. Am. Chem. Soc.* **1967**, *89*, 186–187.
[11] B. S. Chang, S. Oyola-Reynoso, J. Chen, M. Lu, M. M. Thuo, *Polym. Chem.* **2017**, *8*, 3475–3484.
[12] P. G. Arapakos, *J. Am. Chem. Soc.* **1967**, *89*, 6794–6796.
[13] M. Simic, E. Hayon, *Radiat. Res.* **1971**, *48*, 244.
[14] D. Zhu, L. Zhang, R. E. Ruther, R. J. Hamers, *Nat. Mater.* **2013**, *12*, 836–841.
[15] F. S. Dainton, D. M. Wiles, A. N. Wright, *J. Polym. Sci.* **1960**, *45*, 111–118.
[16] K. Lim, B. Fenk, J. Popovic, J. Maier, *ACS Appl. Mater. Interfaces* **2021**, *13*, 51767–51774.
[17] J. Popovic, *Energy Technol.* **2021**, *9*, 2001056.

[18] F. S. Dainton, D. M. Wiles, A. N. Wright, *J. Chem. Soc.* **1960**, *4*, 4283–4289.
[19] Z. Grobelny, A. Stolarzewicz, M. Szczepanski, M. Sokol, *Curr. Org. Chem.* **2008**, *12*, 1040–1049.
[20] F. Cafasso, B. R. Sundheim, *J. Chem. Phys.* **1959**, *31*, 809–813.
[21] C. Tsvetanov, *Makromol. Chem.* **1970**, *134*, 313–316.
[22] A. Stolarzewicz, Z. Grobelny, J. Grobelny, *Spectrochim. Acta Part A* **2000**, *56*, 1257–1265.
[23] J. Grobelny, M. Sokól, Z. J. Jedliński, *Magn. Reson. Chem.* **1991**, *29*, 679–680.
[24] X. Ren, K. C. Lau, M. Yu, X. Bi, E. Kreidler, L. A. Curtiss, Y. Wu, *ACS Appl. Mater. Interfaces* **2014**, *6*, 19299–19307.
[25] T. R. Tuttle, S. I. Weissman, *J. Am. Chem. Soc.* **1958**, *80*, 5342–5344.
[26] Y. Zheng, P. B. Balbuena, *J. Chem. Phys.* **2021**, *154*, 104702.
[27] X. Ren, P. Gao, L. Zou, S. Jiao, X. Cao, X. Zhang, H. Jia, M. H. Engelhard, B. E. Matthews, H. Wu, H. Lee, C. Niu, C. Wang, B. W. Arey, J. Xiao, J. Liu, J.-G. Zhang, W. Xu, *Proc. Natl. Acad. Sci. USA* **2020**, *117*, 28603–28613.

Manuscript received: May 12, 2022
Accepted manuscript online: June 13, 2022
Version of record online: July 5, 2022